



# Specially designed B<sub>4</sub>C/SnO<sub>2</sub> nanocomposite for photocatalysis: traditional ceramic with unique properties

Paviter Singh<sup>1</sup> · Gurpreet Kaur<sup>1</sup> · Kulwinder Singh<sup>1</sup> · Bikramjeet Singh<sup>1</sup> · Manpreet Kaur<sup>1</sup> · Manjot Kaur<sup>1</sup> · Unni Krishnan<sup>1</sup> · Manjeet Kumar<sup>2</sup> · Rajni Bala<sup>3</sup> · Akshay Kumar<sup>1</sup> 

Received: 23 June 2017 / Accepted: 15 January 2018 / Published online: 3 February 2018  
© Springer-Verlag GmbH Germany, part of Springer Nature 2018

## Abstract

Boron carbide: A traditional ceramic material shows unique properties when explored in nano-range. Specially designed boron-based nanocomposite has been synthesized by reflux method. The addition of SnO<sub>2</sub> in base matrix increases the defect states in boron carbide and shows unique catalytic properties. The calculated texture coefficient and Nelson–Riley factor show that the synthesized nanocomposite has large number of defect states. Also this composite is explored for the first time for catalysis degradation of industrial used dyes. The degradation analysis of industrial pollutants such as Novacron red Huntsman (NRH) and methylene blue (MB) dye reveals that the composite is an efficient catalyst. Degradation study shows that 1 g/L catalyst concentration of B<sub>4</sub>C/SnO<sub>2</sub> degrades NRH and MB dye up to approximately 97.38 and 79.41%, respectively, in 20 min under sunlight irradiation. This water-insoluble catalyst can be recovered and reused.

**Keywords** B<sub>4</sub>C/SnO<sub>2</sub> composite · Photocatalyst · Textile dye

## Introduction

Dyes and pigments are extensively used in textile industries, food technology, cosmetics, paper technology, leather and plastic industries for coloring the products. The estimated production of different dyes is about approximately 0.7–7 million tons per year (Christie 2007; Hunger 2003; Husain 2006). The extent of pollution caused by discharge of dyes into the environment is unknown. Use of dyes is the main source of environmental pollution and also becomes a big threat to aquatic life. The removal of dye from wastewater is a crucial need of time for better sustainability, as most of the dyes and their secondary products are carcinogenic or mutagenic and noxious in nature (Edison et al. 2016; Mady et al. 2017).

The various methods were used by researchers to decolorize different dyeing effluents. The industrial wastewater treatment involved different processes such as physical (adsorption) (Kurniawan et al. 2006; Björklund and Li 2017), chemical (ozonation) (Ikhtlaq et al. 2014), biological (Shoener et al. 2014; Zhao and Liu 2016; Norman and Earnshaw 1997) reverse osmosis as well as photocatalysis (Kaur et al. 2016). The high cost of physical as well as chemical methods has failed to treat wastewater, as this comes to be economically unrealistic and also results in unavoidable secondary pollution. The photocatalysis technology is economically viable method used for degradation of dyes at ambient conditions.

Carbides have attracted attention of researchers in recent years due to their extraordinary properties such as high mechanical strength, high melting point and their chemical inertness owing to their potential applications in thermionic electron sources. Nanostructured carbides have been used in various fields such as biomaterials, light weight/high strength materials, high temperature resistant materials, and semi-conducting devices (Jia and Fischer 1996; Chen et al. 2004).

Various synthesis methods have been employed in the synthesis of boron carbide (B<sub>4</sub>C) nanostructures such as carbothermal method from reduction of boron oxide (B<sub>2</sub>O<sub>3</sub>)

✉ Akshay Kumar  
akshaykumar.tiet@gmail.com

<sup>1</sup> Advanced Functional Material Laboratory, Department of Nanotechnology, Sri Guru Granth Sahib World University, Fatehgarh Sahib 140 406, Punjab, India

<sup>2</sup> Department of Electrical Engineering, Incheon National University, Yeonsu-Gu 406 772, South Korea

<sup>3</sup> Department of Mathematics, Punjabi University, Patiala 147 002, Punjab, India

over 1000 °C, thermal decomposition method, gaseous reaction between boron trichloride ( $\text{BCl}_3$ ) and a methane hydrogen mixture in the presence of radio frequency argon plasma, reduction of  $\text{BCl}_3$  by  $\text{CH}_4$  at 1500 °C with laser (Najafi et al. 2012; Wang et al. 2010). A wide range of high temperature synthesis methods can be used for preparation of  $\text{B}_4\text{C}$  nanostructures directly from boron and carbon (Hajizamani and Alizadeh 2012). But these methods are economically not viable due to expensive precursors.

As metal oxides have attracted considerable attraction in research field due to their physical and chemical properties. Among them, tin oxide ( $\text{SnO}_2$ ) has a wide band gap (3.6 eV) and high thermal stability, so  $\text{SnO}_2$  is a potential candidate as a photocatalyst (Wang et al. 2006; Acevedo et al. 2015). The barriers in photocatalytic efficiency in case of  $\text{SnO}_2$  nanoparticles are aggregation and electron hole recombination process.

Transition of metal oxides, phosphides, and sulfides replaced high cost noble metals-based electro-catalysts as well as photo-catalysts in the past years due to their low cost and high activity (Zou and Zhang 2015). Though, corrosion and passivation under acidic conditions cause main hurdle for most of these materials. Besides, there is need of developing a stable and catalytically active material for photocatalysis process in order to reduce water pollution. Transition metal oxides usually showed their failures in the field of active site engineering. In recent years, the catalysts that contain non-metallic nature and earth abundance such as carbon are employed as alternative catalyst materials for water purification process.

Also,  $\text{B}_4\text{C}$  is a semiconductor with band gap of about 1.5 eV (Domnich et al. 2011). The composite of  $\text{SnO}_2$  with  $\text{B}_4\text{C}$  as base matrix can show remarkable photocatalytic properties. Also the catalyst can be recovered and reused.

The present study deals with synthesis and photocatalytic properties of  $\text{B}_4\text{C}/\text{SnO}_2$  nanocomposite.  $\text{B}_4\text{C}/\text{SnO}_2$  composite has been synthesized using wet chemical synthesis method in order to obtain the improved photocatalytic efficiency for wastewater treatment. Industrial pollutants, methylene blue (MB) and Novacron red Huntsman (NRH) dyes, were used as target materials. Their degradation analysis is thoroughly studied and a proposed degradation mechanism in the light of crystal structure is also presented.

## Experimental section

### Materials

Boric acid ( $\text{H}_3\text{BO}_3$ , 99.9%), activated magnesium (Mg, 98%), acetone (used as carbon source),  $\text{SnCl}_2$ , and hydrochloric acid were purchased from Sigma-Aldrich. All

the chemicals were used as received without any further purification.

### Synthesis of $\text{B}_4\text{C}/\text{SnO}_2$ catalyst

$\text{B}_4\text{C}$  nanoparticles were successfully synthesized using solvothermal method (Singh et al. 2014, 2016). The  $\text{B}_4\text{C}/\text{SnO}_2$  photocatalyst was prepared by reflux method. The freshly prepared aqueous solutions of  $\text{SnCl}_2$ ,  $\text{B}_4\text{C}$  and HCl were added to magnetically stirred round bottom flask, respectively, and refluxed at 100 °C for 5 h. The obtained product was cooled to room temperature. The as-prepared sample was collected and washed with distilled water so that neutral pH is obtained. The washed precipitates were collected and dried in vacuum at 80 °C for 6 h.

### Characterization

The dried powder of  $\text{B}_4\text{C}/\text{SnO}_2$  composite was characterized by powder X-ray diffraction (XRD). The XRD pattern with diffraction intensity versus  $2\theta$  was recorded in a Rigaku instrument with  $\text{Cu-K}_\alpha$  radiation ( $\lambda = 1.5418 \text{ \AA}$ ). Transmission Electron Microscope (TEM) was carried out on TECNAI G2 20 FEI at 200 keV in order to study the morphology of synthesized material. Optical absorption spectrums were studied using UV–visible Shimadzu UV-2600 spectrophotometer.

### Photocatalysis experiment

The photocatalytic activities of  $\text{B}_4\text{C}/\text{SnO}_2$  (1 g/L) were evaluated by degradation of aqueous solutions of MB (1 mg/L) dye and a textile dye NRH (1 mg/L). All experiments were carried out at room temperature. The aqueous solutions were magnetically stirred for 30 min in dark to get the adsorption–desorption equilibrium followed by sunlight irradiation. The maximum absorption wavelength of MB was observed at 664 nm. Typically, 20 mg of photocatalyst (1 g/L) was added into 20 mL of 1 mg/L MB and NRH aqueous solution. Analytical samples were taken from reaction systems after specified time period and centrifuged to separate photocatalyst before analysis. The changes in absorption intensity in spectra were studied using UV–visible spectrophotometer. Similar processes were repeated for 0, 0.2 and 0.6 g/L photocatalyst dosages.

## Result and discussion

### XRD analysis

XRD pattern of the synthesized  $\text{B}_4\text{C}/\text{SnO}_2$  composite is shown in Fig. 1a. The collected pattern was compared with

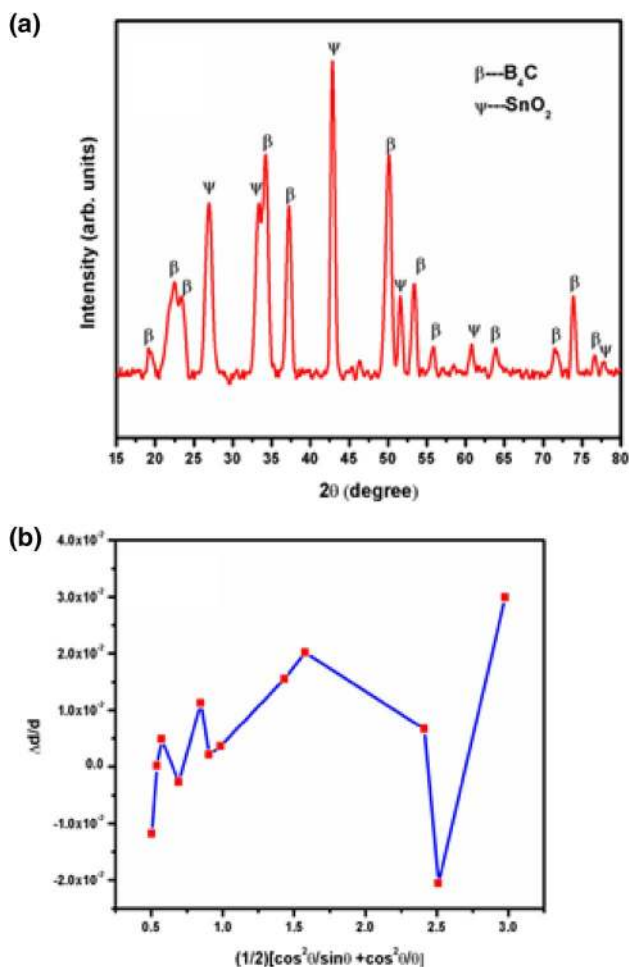


**Fig. 1** **a** XRD pattern, and **b** plot of  $\Delta d/d$  versus Nelson–Riley factor, for synthesized B<sub>4</sub>C/SnO<sub>2</sub> respectively

B<sub>4</sub>C and SnO<sub>2</sub> JCPDS cards, i.e., 35–0798 and 41–1445, respectively. The different diffraction peaks arise from B<sub>4</sub>C and SnO<sub>2</sub>. XRD analysis confirmed the formation of B<sub>4</sub>C and SnO<sub>2</sub> phase in the synthesized sample. The broadening of diffraction peaks was used for the determination of crystallite size. The crystallite size was calculated using Debye–Scherrer formula (Cullity 1978). The calculated average crystallite size of synthesized material is equal to approximately 26 nm.

Further, XRD pattern was used to determine the texture coefficient for synthesized composite. Texture coefficient provides information about preferred growth orientation of the material. The higher the value of texture coefficient of a plane deviated from unit value, the more will be the growth along that particular plane. For the calculation of texture coefficient, standard intensities related to the crystallographic planes were taken from the standard JCPDS cards (35–0798 and 41–1445). Texture coefficient (Kumar et al. 2017, 2015) is calculated using the following relationship:

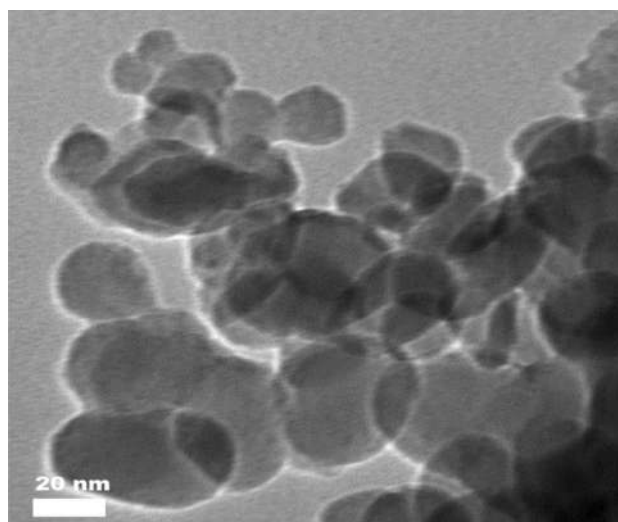


**Fig. 2** TEM image of synthesized B<sub>4</sub>C/SnO<sub>2</sub> nanostructures

$$TC(h_i k_i l_i) = \frac{I(h_i k_i l_i)}{I_0(h_i k_i l_i)} \left[ \frac{1}{n} \sum_{i=1}^n \frac{I(h_i k_i l_i)}{I_0(h_i k_i l_i)} \right]^{-1} \quad (1)$$

where  $TC(hkl)$ ,  $I(hkl)$  and  $I_0(hkl)$  is texture coefficient, experimental and standard intensities of the plane specified by miller indices, respectively. The value of  $n$  represents the number of different peaks.

The texture coefficient analysis reveals that the synthesized material is more grown along (211) with a texture coefficient value 4.513. The growth of the synthesized composite along (211) can be ascribed to the presence of defects in the synthesized sample. Further, the presence of defect states has also been studied from XRD results. The variation of  $\Delta d/d$  with Nelson–Riley factor (Kumar et al. 2015; Singh et al. 2017) is shown in Fig. 1b. The standard values of  $d$  spacing of B<sub>4</sub>C were taken from ICDD card no. 35-0798. It is observed that in case of composite, the scatteredness of  $\Delta d/d$  increased. The scatteredness of  $\Delta d/d$  indicated the large density of defect states present in the samples (Kaur et al. 2007). Therefore, it can be concluded that the SnO<sub>2</sub> incorporation leads to an increase in the defect state density. The effect of defect states or stacking faults in dye degradation has been discussed at the end of this section.

### TEM analysis

TEM image of the as synthesized B<sub>4</sub>C/SnO<sub>2</sub> is shown in Fig. 2. TEM image revealed that the average size of the synthesized particles is ~ 30 nm. Synthesized nanostructures are nearly spherical and agglomerated in nature. The

agglomeration of particles can be ascribed to small crystallite sizes.

### Mechanism followed

The presence of structural defects and distortion in  $B_4C/SnO_2$  influences its structure. These inherent structural defects result in  $B_4C/SnO_2$  with high efficiency in sunlight harvesting and make it a good catalyst for industrial pollutants. Existence of defects causes the downshift in conduction band and available new mid gap states that enable the boron carbide as visible light harvesting material (Liu et al. 2013).

The defects have also shown their impact on carrier relaxation dynamics, resulted in charge separation by trapping electron and holes (Joshi et al. 2010; Klimov et al. 1999; Zhang 2000). Nelson–riley plot as well as texture coefficient indicates the presence of structural defects in  $B_4C/SnO_2$ .  $SnO_2$  can absorb UV wavelength light and results in electron hole separation.  $SnO_2$  makes electron availability to

conduction band of  $B_4C$ . These electrons and holes help to produce the  $\bullet OH$  radicals resulting in degradation of dyes.

### Photocatalysis analysis

The synthesized  $B_4C/SnO_2$  composite, employed as a photocatalyst for the degradation of MB and NRH in water under sunlight irradiation. The effect of concentration loadings of  $B_4C/SnO_2$  catalyst on degradation of dyes was studied. The degradation efficiency of a dye was calculated from change in the concentration of MB and NRH dye using the following formula:

$$\text{Degradation ratio \%} = \frac{C_0 - C_t}{C_0} \times 100 \quad (2)$$

where  $C_0$  and  $C_t$  were the concentrations of dye before and after that reaction. Figures 3a–d and 4a–d show the absorption intensity changes of MB and NRH dyes with different

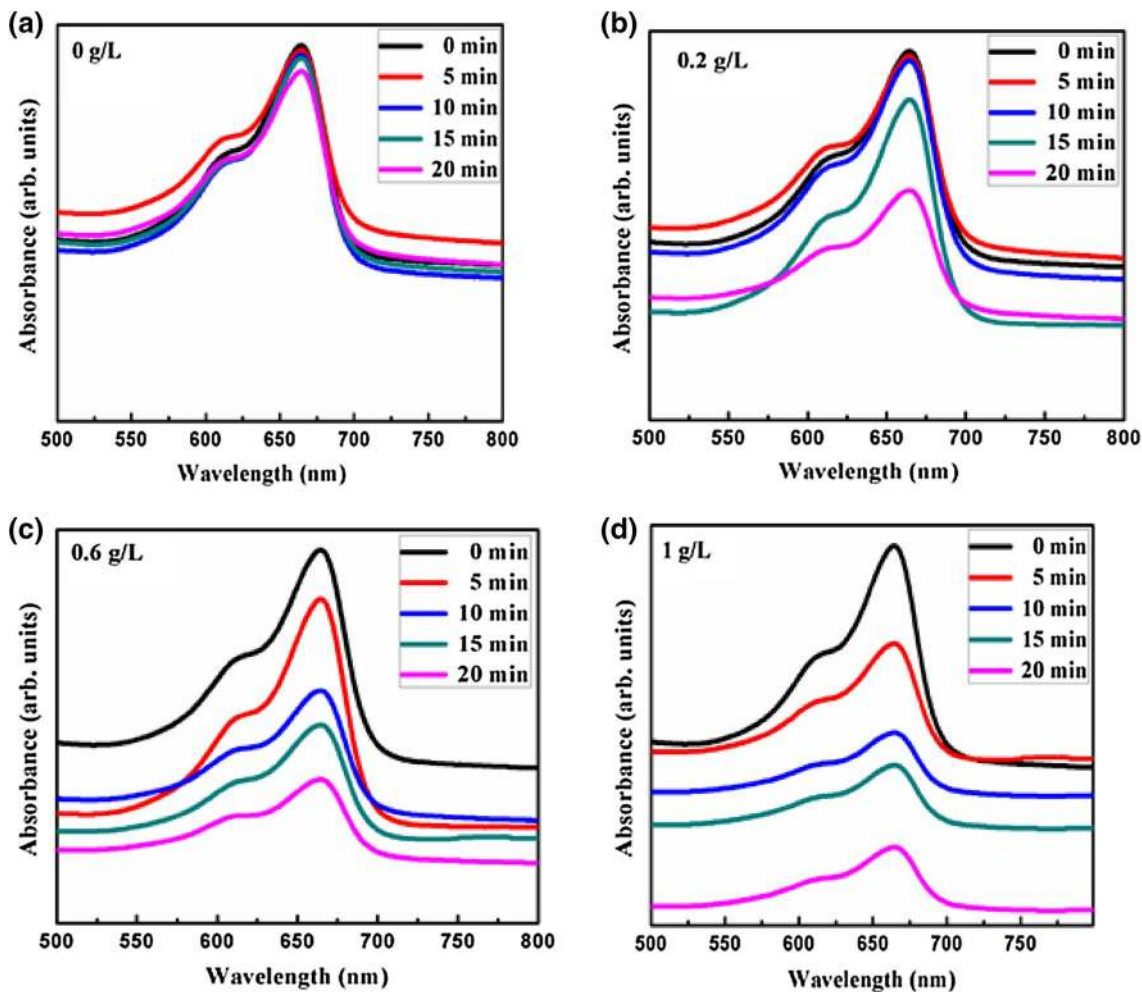


**Fig. 3** a–d Photodegradation plot of organic dye methylene blue dye (1 mg/L) aqueous solution after continuous sunlight irradiation in the presence of  $B_4C/SnO_2$  catalyst loading: (a) 0 g/L, (b) 0.2 g/L, (c) 0.6 g/L, (d) 1 g/L

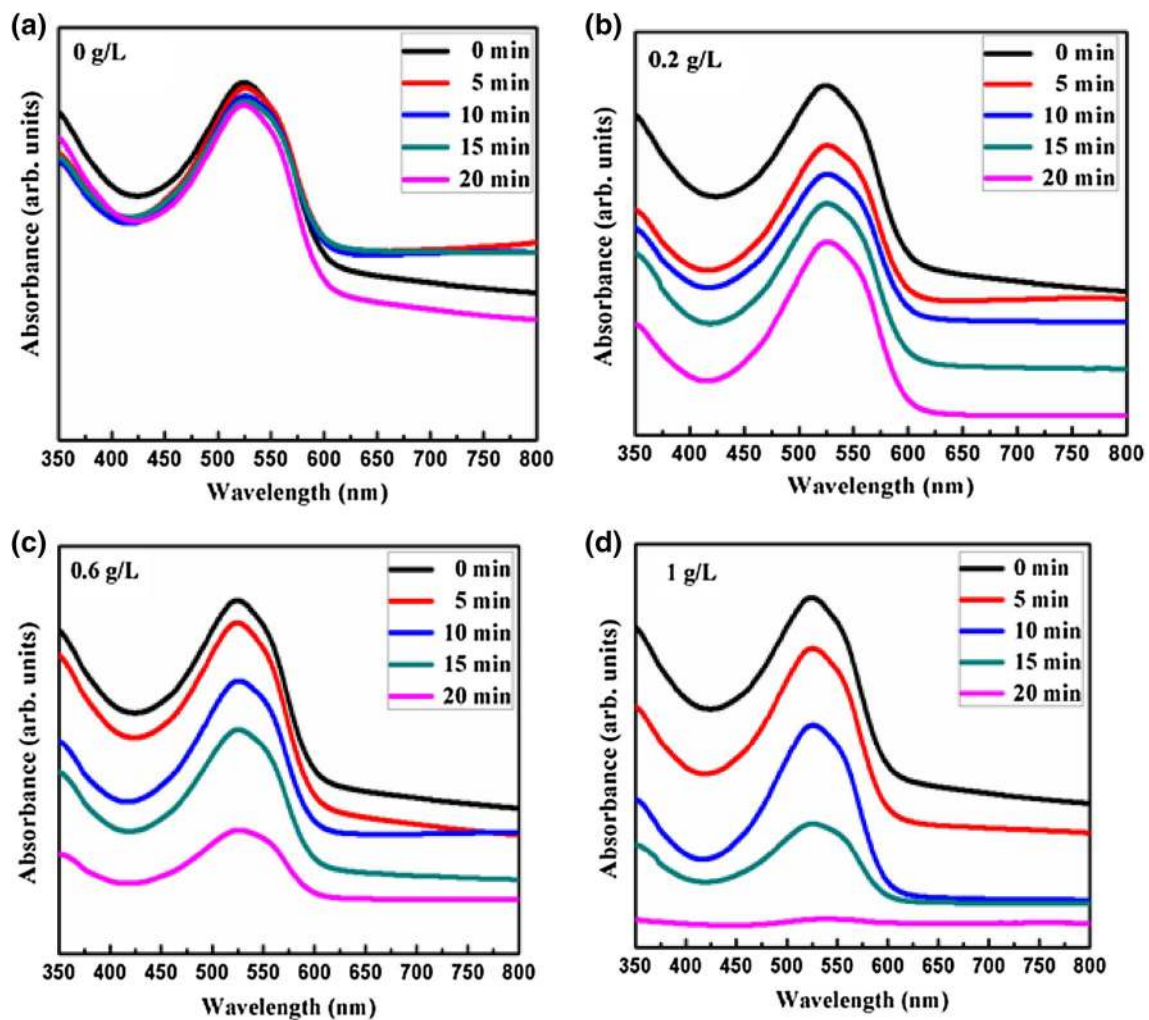


**Fig. 4** a–d Photodegradation plot of textile dye Novacron red dye (1 mg/L) aqueous solution after continuous sunlight irradiation in the presence of  $B_4C/SnO_2$  catalyst loading: (a) 0 g/L, (b) 0.2 g/L, (c) 0.6 g/L, (d) 1 g/L

**Table 1** Degradation ratio of MB dye and a textile dye NRH with different catalyst dose of  $B_4C/SnO_2$ , respectively

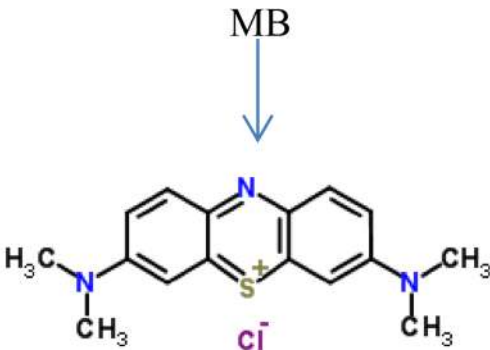
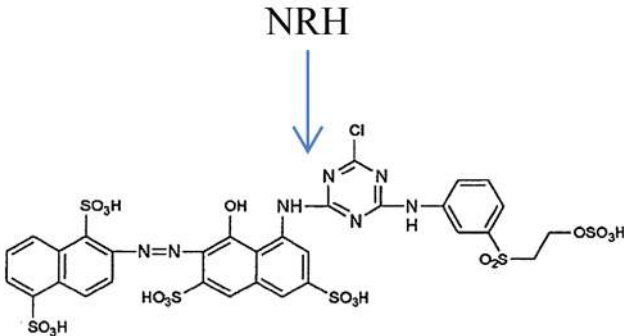
Dye/concentration (1 mg/L)	Concentration of $B_4C/SnO_2$ catalyst loading (g/L)	Degradation efficiency (%)
Methylene blue (MB)	1	79.41
	0.6	61.42
	0.2	37.76
	0	6.969
Novacron red Huntsman (NRH)	1	97.38
	0.6	68.89
	0.2	47.38
	0	6.686

concentration of catalyst (0 to 1 g/L) under sunlight irradiation for homogeneous time interval of 20 min which

specifies the degradation of dye, respectively. The removal efficiency of MB and NRH with different concentration of  $B_4C/SnO_2$  catalyst is described in Table 1. Basic characteristics of MB dye and a textile dye NRH are given in Table 2. Methylene blue has absorption peak at 664 nm and a shoulder at 610 nm. The intensity of both absorption bands get reduced as sunlight irradiation time increases. This indicates the decomposition or degradation of chromo-phoric group of dye into simple intermediate smaller molecular sized molecules. On the other hands, NRH dye has a strong absorption band at 524 nm as shown in Fig. 4. The absorption peak intensity declined as time of sunlight irradiation increased from 0 to 20 min (Fig. 4a–d).

Figure 5a represents the degradation efficiency of  $B_4C/SnO_2$  catalyst for degradation of MB dye. The methylene blue degradation efficiency is enhanced approximately up

**Table 2** Basic characteristics of MB dye and a textile NRH dye

Chemical name	Methylene blue	Novacron red Huntsman
Chemical formula	C <sub>16</sub> H <sub>18</sub> ClN <sub>3</sub> S	C <sub>18</sub> H <sub>14</sub> N <sub>2</sub> Na <sub>2</sub> O <sub>8</sub> S <sub>2</sub>
Molecular weight (g/mol)	~ 319.85	~ 496.46
λ <sub>max</sub> (nm)	664	524
Abbreviated name	MB	NRH
Chemical structure		

to 79.41% for 1 g/L B<sub>4</sub>C/SnO<sub>2</sub> catalyst under sunlight than other concentrations of B<sub>4</sub>C/SnO<sub>2</sub> photocatalyst.

The average decolourization rate for different catalyst loading in MB dye was calculated using Eq. 3 and is presented as a bar graph in Fig. 5b.

$$\text{Average degradation rate} = \frac{C \times D\% \times 1000}{100 \times t} \quad (3)$$

where *C* and *D* % are the initial concentrations of dye solution and degraded dye after time *t*, respectively.

The average degradation rate of MB dye with 1 g/L B<sub>4</sub>C/SnO<sub>2</sub> catalyst is calculated as ~ 5.0425% (Fig. 5b). The half-life of a dye is defined as a time at which its concentration became half which was calculated using intersection curve of *C/C*<sub>0</sub> (MB concentration) and 1-*C/C*<sub>0</sub> (degradation efficiency) that was estimated approximately as 8.08 min (Fig. 5c).

Degradation efficiency for NRH dye via 1 g/L B<sub>4</sub>C/SnO<sub>2</sub> catalyst loading is estimated to be approximately 97.38% (Fig. 6a), i.e., an excellent performance of B<sub>4</sub>C/SnO<sub>2</sub>

catalyst, under sunlight irradiation. The average degradation rate via different concentration of B<sub>4</sub>C/SnO<sub>2</sub> catalyst for NRH dye was displayed as bar graph representation in Fig. 6b. The average degradation rate of NRH dye was calculated (using Eq. 3) as 43.82%. As the concentration of catalyst increased, the decrease in half-life was observed (Kaur et al. 2017). The half-life of NRH dye was estimated as 11.81 min shown in Fig. 6c.

## Conclusion

B<sub>4</sub>C/SnO<sub>2</sub> composite synthesized by simple reflux method has been employed as a catalyst for degradation of an organic and a textile dye, i.e., MB and NRH under sunlight irradiation, respectively. The composite acts as an efficient photocatalyst due to the presence of defect states for the removal of industrial pollutants that are noxious to the humans as well as marine life. The effect of concentration of composite as catalyst on degradation under

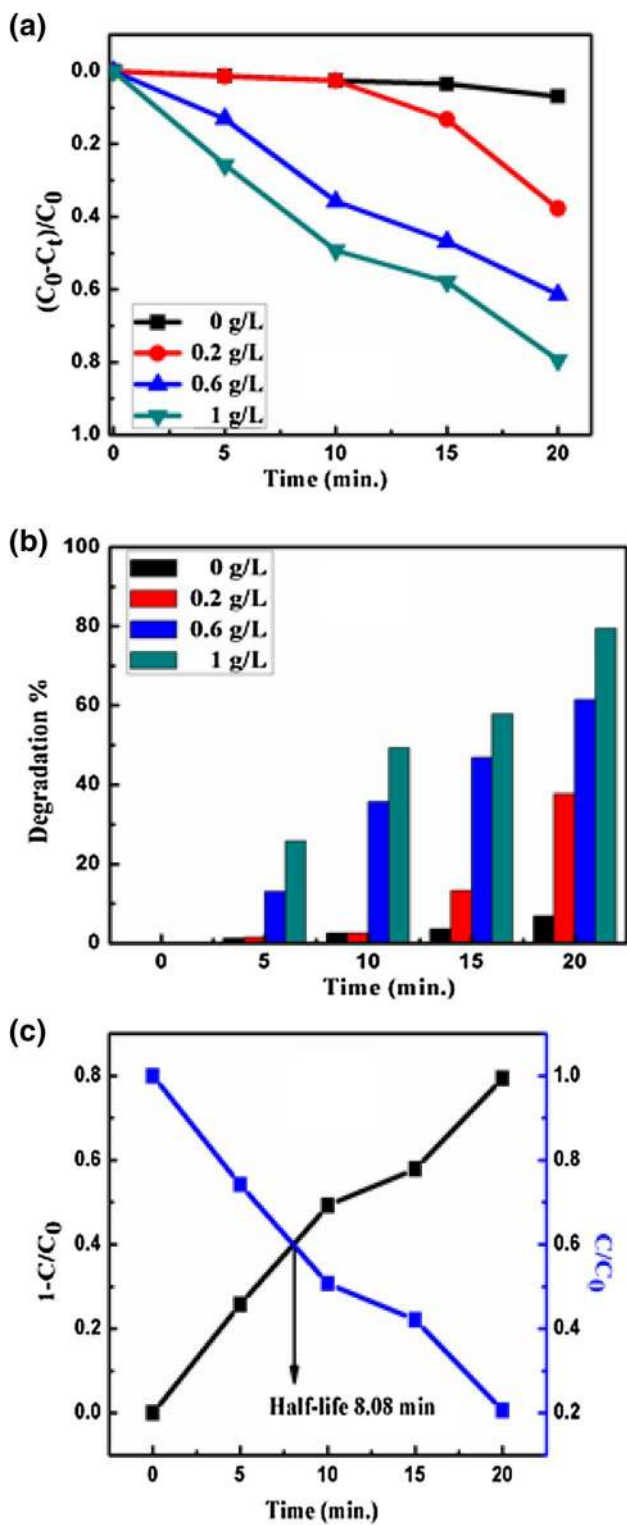


**Fig. 5** **a** Degradation efficiency of  $B_4C/SnO_2$  catalyst with aqueous dispersion of methylene blue (MB) dye as function of irradiation time, **b** average degradation rate of different concentrations of catalyst  $B_4C/SnO_2$  for methylene blue (MB) at uniform time interval under sunlight irradiation, **c** half-life dye estimation curve from  $C/C_0$  and degradation efficiency  $1-C/C_0$  for 1 g/L of  $B_4C/SnO_2$  catalyst loading in methylene blue dye

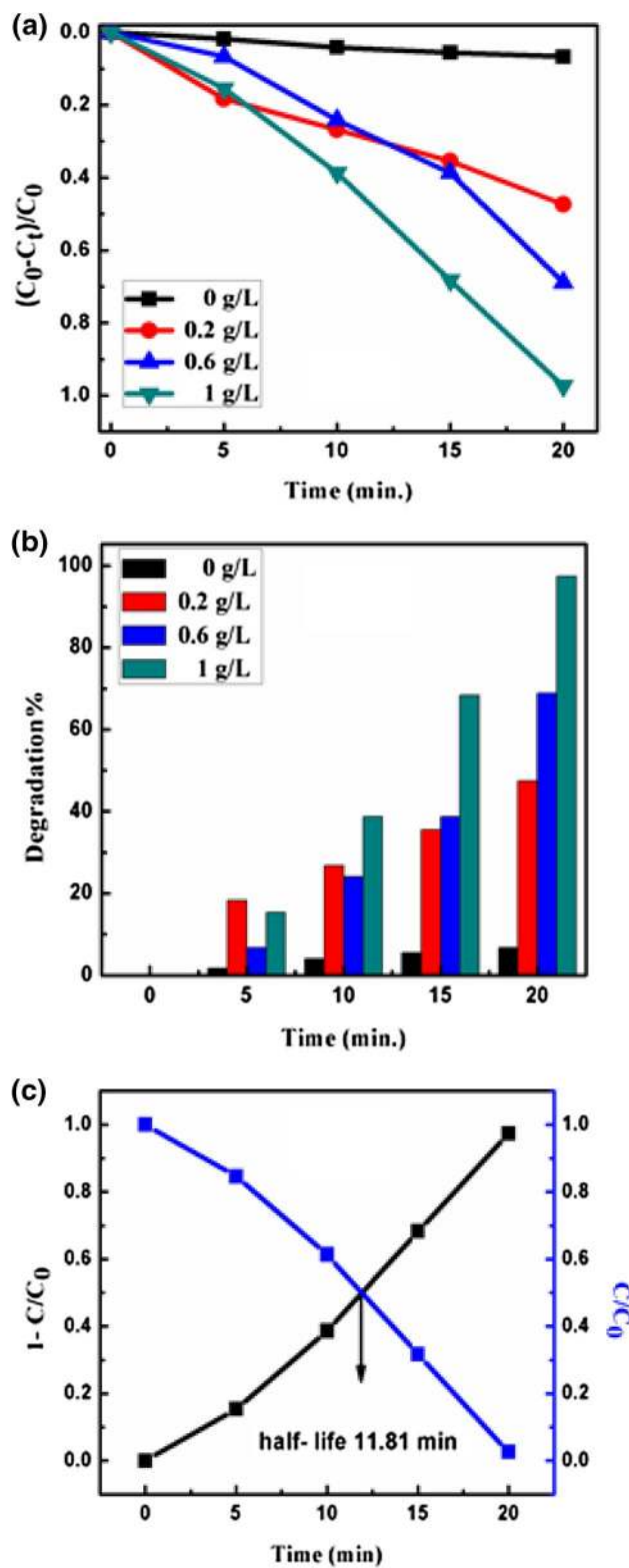


**Fig. 6** **a** Photocatalytic degradation efficiency of different concentrations of  $B_4C/SnO_2$  catalyst loading to Novacron red Huntsman dye, **b** Average degradation rate of different concentration of catalyst  $B_4C/SnO_2$  for Novacron red Huntsman dye (NRH) at uniform time interval under sunlight irradiation, **c** Half-life dye estimation curve from  $C/C_0$  and degradation efficiency  $1-C/C_0$  for 1 g/L of  $B_4C/SnO_2$  catalyst loading in Novacron red dye

sunlight irradiation was studied. For 1 g/L  $B_4C/SnO_2$  catalyst, degradation efficiency of about 79.41% was achieved with MB dye under sunlight irradiation in 20 min. The catalyst  $B_4C/SnO_2$  with the dosage of 1 g/L competently degrades the NRH dye (1 mg/L) with 97.38%. The unique catalytic properties of  $B_4C/SnO_2$  make it an alternative material in the field of photocatalysis.

**Acknowledgements** This work was funded by Board of Research in Nuclear Sciences, Department of Atomic Energy (DAE), India under project no. 34/14/41/2014-BRNS. This work was also supported by DST project No. EMR/2016/002815.

## References

- Acevedo MC, Stone ML, Schmidt JR, Thomas JG, Ding Q, Chang HC, Tsai ML, He JH, Jin S (2015) Efficient hydrogen evolution catalysis using ternary pyrite-type cobalt phosphosulphide. *Nat Mater* 14:1245. <https://doi.org/10.1038/NMAT4410>
- Björklund K, Li LY (2017) Adsorption of organic stormwater pollutants onto activated carbon from sewage sludge. *J Environ Manag* 197:490–497. <https://doi.org/10.1016/j.jenvman.2017.04.011>
- Chen S, Wang DZ, Huang JY, Ren ZF (2004) Synthesis and characterization of boron carbide nanoparticles. *Appl Phys A Mater Sci Process* 79:1757–1759. <https://doi.org/10.1007/s00339-004-2913-6>
- Christie RM (2007) Environmental aspects of textile dyeing. Woodhead, Boca Raton/Cambridge
- Cullity BD (1978) Elements of X-ray Diffraction. Addison-Wesley, New York
- Domnich V, Reynaud S, Haber RA, Chhowalla M (2011) Boron carbide: structure, properties, and stability under stress. *J Am Ceram Soc* 94(11):3605–3628. <https://doi.org/10.1111/j.1551-2916.2011.04865.x>
- Edison TNJI, Atchudan R, Sethuraman MG, Rok Lee Yong (2016) Reductive-degradation of carcinogenic azo dyes using Anacardium occidentale testa derived silver nanoparticles. *J Photochem Photobiol, B* 162:604–610. <https://doi.org/10.1016/j.jphotobiol.2016.07.040>
- Hajizamani M, Alizadeh A (2012) Deposition of a  $Ni_3P$  nano-scale layer on  $B_4C$  nanoparticles by simple electroless plating in an acidic bath. *Appl Nanosci* 2(4):417–421. <https://doi.org/10.1007/s13204-011-0055-7>
- Hunger K (2003) Industrial dyes: chemistry, properties, applications. Wiley-VCH, Weinheim/Cambridge
- Husain Q (2006) Potential applications of the oxidoreductive enzymes in the decolorization and detoxification of textile and other synthetic dyes from polluted water: a review. *Crit Rev Biotechnol* 26:201–221. <https://doi.org/10.1080/07388550600969936>
- Ikhlaiq A, Brown DR, Hordern BK (2014) Catalytic ozonation for the removal of organic contaminants in water on ZSM-5 zeolites. *Appl Catal B* 154–155:110–122. <https://doi.org/10.1016/j.apcatb.2014.02.010>
- Jia K, Fischer TE (1996) Abrasion resistance of nanostructured and conventional cemented carbides. *Wear* 200:206–214. [https://doi.org/10.1016/S0043-1648\(96\)07277-8](https://doi.org/10.1016/S0043-1648(96)07277-8)
- Joshi UA, Palasyuk A, Arney D, Maggard PA (2010) Semiconducting oxides to facilitate the conversion of solar energy to chemical fuels. *J Phys Chem Lett* 1:2719–2726. <https://doi.org/10.1021/jz100961d>
- Kaur J, Roy SC, Bhatnagar MC (2007) Highly sensitive  $SnO_2$  thin film  $NO_2$  gas sensor operating at low temperature. *Sens Actuators B* 123:1090–1095. <https://doi.org/10.1016/j.snb.2006.11.031>
- Kaur G, Singh B, Singh P, Kaur M, Buttar KK, Thakur A, Bala R, Kumar M, Kumar A (2016) Preferentially grown nanostructured iron disulphide ( $FeS_2$ ) for removal of industrial pollutants. *RSC Adv* 6:99120–99128. <https://doi.org/10.1039/c6ra18838a>
- Kaur G, Singh B, Singh P, Singh K, Thakur A, Kumar M, Bala R, Kumar A (2017) Iron disulfide ( $FeS_2$ ): a promising material for removal of industrial pollutants. *Chem Sel* 2:2166–2173. <https://doi.org/10.1002/slct.201700087>
- Klimov VI, McBranch DW, Leatherdale CA, Bawendi MG (1999) Electron and hole relaxation pathways in semiconductor quantum dots. *Phys Rev B* 60(19):13740–13749. <https://doi.org/10.1103/PhysRevB.60.13740>
- Kumar M, Kumar A, Abhyankar AC (2015a) Occurrence of non-equilibrium orthorhombic  $SnO_2$  phase and its effect in preferentially grown  $SnO_2$  nanowires for CO detection. *RSC Adv* 5:35704–35708. <https://doi.org/10.1039/c4ra15539d>
- Kumar M, Singh B, Yadav P, Bhatt V, Kumar M, Singh K, Abhyankar AC, Kumar A, Yun JH (2015b) Effect of structural defects, surface roughness on sensing properties of Al doped ZnO thin films deposited by chemical spray pyrolysis technique. *Ceram Int* 43:3562–3568. <https://doi.org/10.1016/j.ceramint.2016.11.191>
- Kumar V, Singh K, Kumar A, Kumar M, Singh K, Vij A, Thakur A (2017) Effect of solvent on crystallographic, morphological and optical properties of  $SnO_2$  nanoparticles. *Mater Res Bull* 85:202–208. <https://doi.org/10.1016/j.materresbull.2016.09.020>
- Kurniawan TA, Chan GY, Lo WH, Babel S (2006) Physico-chemical treatment techniques for wastewater laden with heavy metals. *Chem Eng J* 118:83–98. <https://doi.org/10.1016/j.cej.2006.01.015>
- Liu J, Wen S, Hou Y, Zuo F, Beran GJO, Feng P (2013) Boron carbides as efficient, metal free, visible-light-responsive photocatalysts. *Angew Chem Int Ed* 52:1–6. <https://doi.org/10.1002/anie.201209363>
- Mady AH, Baynosa ML, Tuma D, Shim JJ (2017) Facile microwave-assisted green synthesis of  $Ag-ZnFe_2O_4@rGO$  nanocomposites for efficient removal of organic dyes under UV- and visible-light irradiation. *Appl Catal Environ* 203:416–427. <https://doi.org/10.1016/j.apcatb.2016.10.033>
- Najafi A, Golestani-Fard F, Rezaie HR, Ehsani N (2012) A novel route to obtain  $B_4C$  nano powder via sol-gel method. *Ceram Int* 38:3583–3589. <https://doi.org/10.1016/j.ceramint.2011.12.074>
- Norman GN, Earnshaw Alan (1997) Chemistry of the Elements. Butterworth-Heinemann, ISBN, p 0080379419
- Shoener B, Bradley I, Cusick R, Guest J (2014) Energy positive domestic wastewater treatment: the roles of anaerobic and phototrophic technologies. *Environ Sci* 16:1204–1222. <https://doi.org/10.1039/C3EM00711A>
- Singh P, Singh B, Kumar M, Kumar A (2014) One step reduction of boric acid to boron carbide nanoparticles. *Ceram Int* 40:15331–15334. <https://doi.org/10.1016/j.ceramint.2014.06.101>
- Singh P, Kaur M, Singh B, Kaur G, Kumar M, Bala R, Kumar A (2016) Gap state related blue light emitting boron-carbon core shell structures. *AIP Conf Proc* 1728:020690. <https://doi.org/10.1063/1.4946741>
- Singh P, Singh K, Kaur M, Kaur H, Singh B, Kaur G, Kaur M, Kumar M, Kaur K, Bala R, Kumar A (2017) Preferentially grown nanostructured  $MgB_2C_2$ : a new material for lightning applications. *Superlattices Microstruct* 103:1–8. <https://doi.org/10.1016/j.spmi.2017.01.013>



- Wang G, Lu W, Li JH, Choi JY, Jeong Y, Choi SY, Park JB, Ryu MK, Lee K (2006) V-shaped tin oxide nanostructures featuring a broad photocurrent signal: an effective visible-light-driven photocatalyst. *Small* 2:1436. <https://doi.org/10.1002/sml.200600216>
- Wang HJ, Sun FQ, Zhang Y, Li LS, Chen HY, Wu QS, Yu JC (2010) Photochemical growth of nanoporous SnO<sub>2</sub> at the air–water interface and its high photocatalytic activity. *J Mater Chem* 20:5641–5645. <https://doi.org/10.1039/b926930d>
- Zhang JZ (2000) Interfacial charge carrier dynamics of colloidal semiconductor nanoparticles. *J Phys Chem B* 104(31):7239–7253. <https://doi.org/10.1021/jp000594s>
- Zhao Q, Liu Y (2016) State of the art of biological processes for coal gasification wastewater treatment. *Biotechnol Adv* 34:1064–1072. <https://doi.org/10.1016/j.biotechadv.2016.06.005>
- Zou X, Zhang Y (2015) Noble metal-free hydrogen evolution catalysts for water splitting. *Chem Soc Rev* 44:5148. <https://doi.org/10.1039/c4cs00448e>

**Publisher's Note** Springer Nature remains neutral with regard to jurisdictional claims in published maps and institutional affiliations.